Distribution Agreement

In presenting this thesis as a partial fulfillment of the requirements for a degree from Emory University, I hereby grant to Emory University and its agents the non-exclusive license to archive, make accessible, and display my thesis in whole or in part in all forms of media, now or hereafter know, including display on the World Wide Web. I understand that I may select some access restrictions as part of the online submission of this thesis. I retain all ownership rights to the copyright of the thesis. I also retain the right to use in future works (such as articles or books) all or part of this thesis.

Chinar Sanghvi April 19, 2011

Synthesis, characterization, and *in vitro* biological testing of gold(III) polypyridyl compounds: Insights into cytotoxicity of neutral distorted square pyramidal complexes

by

Chinar Sanghvi

Dr. Cora MacBeth
Adviser

Department of Chemistry

Dr. Cora MacBeth

Adviser

Dr. Nitya Jacob

Committee Member

Dr. Brian Dyer

Committee Member

April 19, 2011

Synthesis, characterization, and *in vitro* biological testing of gold(III) polypyridyl compounds: Insights into cytotoxicity of neutral distorted square pyramidal complexes

By

Chinar Sanghvi

Dr. Cora MacBeth

Adviser

An abstract of
a thesis submitted to the Faculty of Emory College of Arts and Sciences
of Emory University in partial fulfillment
of the requirements of the degree of Bachelor of Science
with Honors

Department of Chenistry

2011

Abstract

Synthesis, characterization, and *in vitro* biological testing of gold(III) polypyridyl compounds: Insights into cytotoxicity of neutral distorted square pyramidal complexes

By Chinar Sanghvi

In an effort to discover potential metallotherapeutic alternatives to the chemotherapy drug *cis*-platin, two classes of gold(III) coordination complexes have been synthesized and characterized: 1) neutral square pyramidal complexes with 2,9-disubstituted phenanthroline ligands ([(^{R}phen)$AuCl_3$]) and 2) complex ions comprised of protonated phenanthroline ligands and gold tetrachloride anions ([^{R}phenH][$AuCl_4$]). A novel neutral gold(III) 6,6'-dimethyl bipyridine complex also in a square pyramidal geometry ([(^{methyl}bipy)$AuCl_3$]) has also been synthesized and characterized to probe the effect of differing aromatic character of the ligand on solution stability, tumor cell cytotoxicity, and DNA binding. Therefore, all three classes of compounds ([(^{R}phen)$AuCl_3$], [^{R}phenH][$AuCl_4$], and [(^{methyl}bipy)$AuCl_3$]) were assessed for stability against the biological reductants ascorbic acid and glutathione, with the neutral gold(III) phenanthroline complex exhibiting the most stability. Furthermore, these complexes were tested for cytotoxic effects against existing lung and head and neck tumor cell lines. Both the [^{R}phenH][$AuCl_4$] salts and the neutral coordination complexes ([(^{R}phen)$AuCl_3$] were found to be more cytotoxic than *cis*-platin against a number of cancer cell lines whereas [(^{methyl}bipy)$AuCl_3$] was more potent than *cis*-platin against only one cancer cell line. These compounds were also examined for DNA binding. The [(^{methyl}bipy)$AuCl_3$] complex displayed only partial DNA binding, suggesting that DNA binding may not be the primary requirement for cancer cell death. Also, protein marker expressions of tumor cell lines treated with [($^{sec\text{-}butyl}$phen)$AuCl_3$] were analyzed and it was ascertained that the induction of cytotoxicity occurs via a progressive mechanism with increasing concentrations of the drug: from cell cycle arrest to autopahgy to

apoptosis. Since the DNA binding and antiproliferative mechanisms of these complexes are found to initiate tumor cell death via a different mechanism than *cis*-platin, they may have utility in treating *cis*-platin-resistant tumor cell lines and alleviating some of the mutagenic side effects associated with *cis*-platin.

Synthesis, characterization, and *in vitro* biological testing of gold(III) polypyridyl compounds:

Insights into cytotoxicity of neutral distorted square pyramidal complexes

By

Chinar Sanghvi

Dr. Cora MacBeth

Adviser

A thesis submitted to the Faculty of Emory College of Arts and Sciences
of Emory University in partial fulfillment
of the requirements of the degree of Bachelor of Sciences
with Honors

Department of Chemistry

2011

Acknowledgements

This research was made possible by funds from the Howard Hughes Medical Institute Grant No. 52005873, the Emory University Research Council, the Oxford College Research Scholars Program, the Pierce Institute for Leadership and Community Engagement), and a donation for cancer research from an Oxford College benefactor. Furthermore, I would like to thank the Oxford College Department of Chemistry, the Emory University Department of Chemistry, the Summer Undergraduate Research Program at Emory, and the Scholarly Inquiry and Research at Emory program for their support and funding for this research.

Several other people have been vital to the completion of this project. I would like to thank Zachary D. Hudson and Melody A. Rhine for their guidance and help with the synthesis of the 2,9-disubstituted phenanthroline gold(III) complexes and salts. I would also like to thank Drs. Georgia Chen, Bruce Peng, and Dongshing Wang for not only providing us with the cytotoxicity assays but also giving me the opportunity to work in their lab this year to obtain the Western blot results and their immense help with all of the cell culture procedures. Furthermore, I would like to thank Dr. Kenneth Hardcastle for solving the crystal structures.

Most importantly, I would like to thank my research mentors, Dr. Cora MacBeth and Dr. Jack Eichler. This research would not have been possible without their mentorship and guidance. I have been truly privileged to work with both of them and they have been the most remarkable mentors. They have helped me both academically and personally and given me such useful guidance over the past 3 years. They have showed me how exhilarating and challenging research can be and their enthusiasm and dedication has been crucial for this project.

Table of Contents

Introduction:

Metallotherapeutic drug design represents a significant area of anti-cancer research, with *cis*-platin (*cis*-diamminedichloroplatinum) (Figure 1) and its platinum(II) analogues being the most successful by-products of this prolonged study. *Cis*-platin has been effectively utilized in the treatment of a variety of cancers, such as ovarian, testicular, and head and neck cancers.[1,2] *Cis*-platin induces cancer cell death via binding to the DNA, distorting the structural features of DNA, and affecting DNA replication and transcription.[3] Although *cis*-platin has been one of the most commonly used metal-based chemotherapy drugs, it has some major drawbacks: 1) the development of resistant tumor lines due to increased effectiveness of biological reductants (glutathione can render the drug inactive) and/or cellular DNA repair mechanisms,[4] 2) exhibition of significant nephrotoxicity and neurotoxicity, and 3) the lack of therapeutic specificity and consequent adverse effects on healthy tissues that have high rates of cell proliferation (bone marrow, hair follicles, gastrointestinal, etc.).[5,6,7]

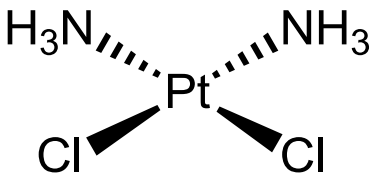

Figure 1. Structure of c*is*-platin

In an effort to minimize the negative side-effects associated with *cis*-platin, alternative metal-based drugs have long been pursued. Specifically, the synthesis of gold therapies has garnered significant attention by a number of research groups.[8,9,10] Initial interest in gold compounds stemmed from their use in the treatment of rheumatoid arthritis with patients undergoing these treatments exhibiting decreased risk of several types of malignancies.[11] In

addition, the gold(III) therapies had been selected for anti-cancer research due to similarities in their molecular character to platinum(II). Gold(III) compounds are isoelectronic to platinum(II) compounds; both possess d^8 outer shell electronic configurations. Therefore, it was believed that the mechanism of cancer cell cytotoxicity for gold (III) compounds would be analogous to *cis*-platin, that is, thru DNA binding and disruption of DNA replication (Figure 2).[12]

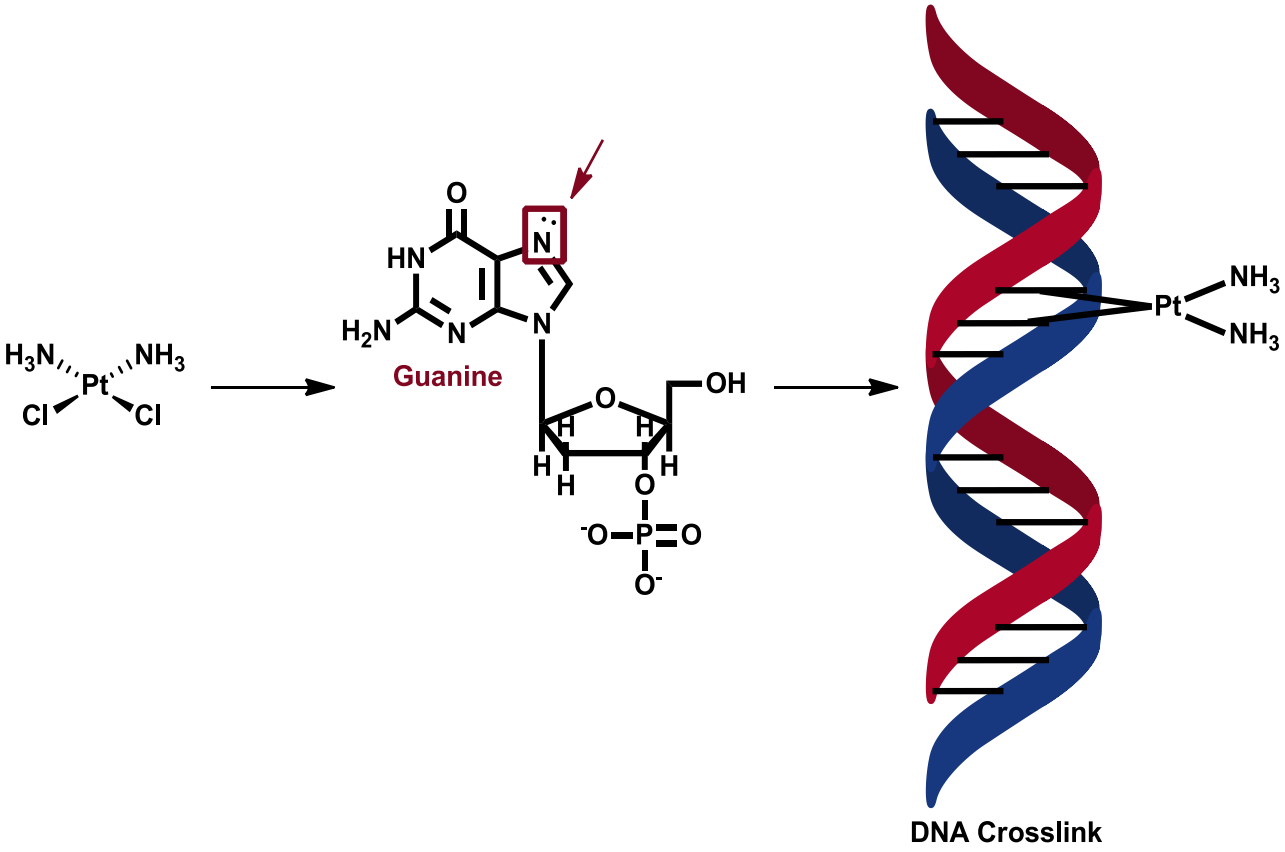

Figure 2. Mechanism of *cis*-platin - DNA binding via the guanine N7 position. Figure adapted from Wang et. al.[13]

However, the DNA binding of gold(III) complexes has been found to be weaker than that of *cis*-platin[8] and subsequent studies have suggested that the therapeutic effect of gold compounds may arise from interactions with the mitochondrial enzyme thioredoxin reductase (TrxR),[14] or through disruption of cellular proteasome activity.[10] Even so, gold compounds possess cytotoxic potentials comparable to and even greater than those of *cis*-platin against a

variety of tumor cell lines. In fact, these alternative mechanisms may explain the cytotoxic effects of gold(III) compounds against *cis*-platin-resistant cell lines and may provide an opportunity for gold(III) therapeutics to alleviate the side-effects associated with *cis*-platin.[15,9]

Not only can the competence of anti-cancer drugs be correlated to their cellular target, but further classification of these drugs can be determined based on the cell death pathway or cell cycle arrest induced. Normal cells have three different cell death mechanisms: 1) apoptosis, 2) necrosis, and 3) autophagy. Apoptosis is a programmed cell death mechanism, where this pathway can be genetically regulated. During stressful conditions, apoptosis can be lead to irreversible shrinking of the cell, bulging of certain portions of the plasma membrane, chromatin condensation, depletion of mitochondrial membrane potential, and nuclear fragmentation. Necrosis has often been referred to as an accidental cell death pathway, usually occurring during ischemic conditions (restricted blood supply) or via exposure to environments deviating from physiological conditions. Common morphological characteristics associated with necrosis include swelling of the cell and organelles, plasma membrane disintegration, and release of proteosomes from lysosomes, leading to cell breakdown. On the other hand, autophagy can initially seem like a survival mechanism where cells obtain energy by digesting their organelles and macromolecules when subject to growth or nutrient depravation. However, upon exposure for longer time periods, the cells undergo autophagy – induced cell death. Most chemotherapeutic drugs, including *cis*-platin, induce apoptosis in cancer cells.[16] Therefore, drugs that induce a different cell death pathway or cell cycle arrest may provide an alternative avenue of cytotoxicity. This varied means of cancer cell attack could provide another approach to curtail the negative side-effects associated with *cis*-platin. Therefore, exploration of the cancer cell

death pathway induced by gold(III) complexes is of paramount importance in discerning their proficiency as anti-cancer therapeutics.

Early exploration into the synthesis of gold(III) coordination complexes yielded drugs with low stability under physiological conditions, a property which could be a significant hindrance to their potency as anti-cancer therapeutics.[17] Similar to *cis*-platin, these initial gold(III) compounds could be reduced to gold(I) and metallic gold *in vivo*, decreasing their success as potential drugs.[18,4] However, recent studies have shown that polydentate ligands, especially those with nitrogen atoms as donor groups, can stabilize the gold(III) center in cellular environments.[19] Shown below are some gold complexes with high solution stability and anti-cancer potential (Figure 3).[17,18]

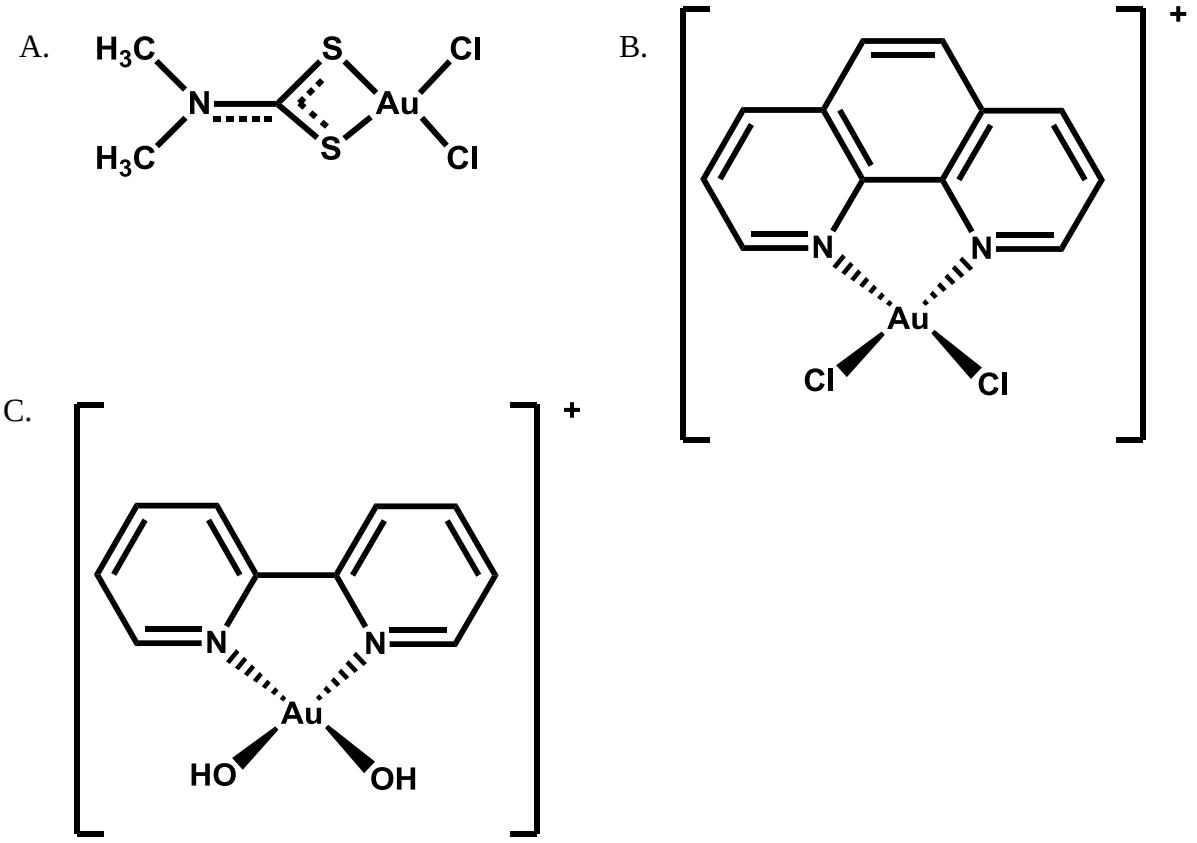

Figure 3. Structure of A. [Au(N,N- dimethyldithiocarbamate)Cl_2], B. [Au(phenanthroline)$(Cl)_2]^+$ and C. [Au(bipyridine)$(OH)_2]^+$.[18,19]

Gold(III) complexes with phenanthroline ligands hold promise as optimal anticancer therapeutics. This is not only due to the stability that the ligand can offer the metal center against reduction but also a result of the fact that phenanthroline coordination complexes with other metals such as lanthanum, palladium, and rhodium have been found to exhibit significant in vitro anti-cancer activity.[20,21,22] However, there is a dearth of structurally characterized gold(III) phenanthroline (phen) compounds. Specifically, only one example of a gold(III) complex with a 2,9-di-substituted phen ligand ([(2,9-dimethylphen)$AuCl_3$], or DMP-gold)[23] had been structurally characterized prior to our recent report.[24] Since phen coordination complexes possess chemotherapeutic potential, we initially sought to synthesize 2,9-dialkylphen (^{R}phen) gold (III) complexes with bulkier ligand substituents. These substitutions were hypothesized to protect the gold(III) center from attack by biological reductants such as glutathione and ascorbic acid by providing steric protection and/or reduction stability. Employing the nucleophilic aromatic addition reaction reported by Pallenberg, *et al.*,[25] we were able to synthesize 2,9-dialkylphen ligands. A subsequent reaction with $HAuCl_4$ resulted in the formation of complex ions comprised of protonated phenanthroline ligands and gold tetrachloride anions ([^{R}phenH][$AuCl_4$]; compounds **1** and **2** in Scheme 1A).[24] In order to obtain direct coordination of the ^{R}phen ligand to the gold(III) metal center, we carried out an alternative reaction with $NaAuCl_4$ and a silver(I) salt that yielded neutral square pyramidal complexes possessing ^{R}phen ligands ([(^{R}phen)$AuCl_3$]; compounds **3** and **4** in Scheme 1B).[16] Having developed a systematic method for preparing gold(III) coordination complexes with ^{R}phen ligands, we attempted to synthesize analogous gold(III) complexes possessing 6,6'-disubstituted bipyridine (^{R}bipy) ligands. This study will report the synthesis and characterization of the neutral gold(III) complex possessing the ^{methyl}bipy ligand ([(^{methyl}bipy)$AuCl_3$]; compound **5** in Scheme 1C), as well as the

in vitro cytotoxicity, DNA binding, and non-cellular reduction stability of compounds **1**, **4**, and **5**.

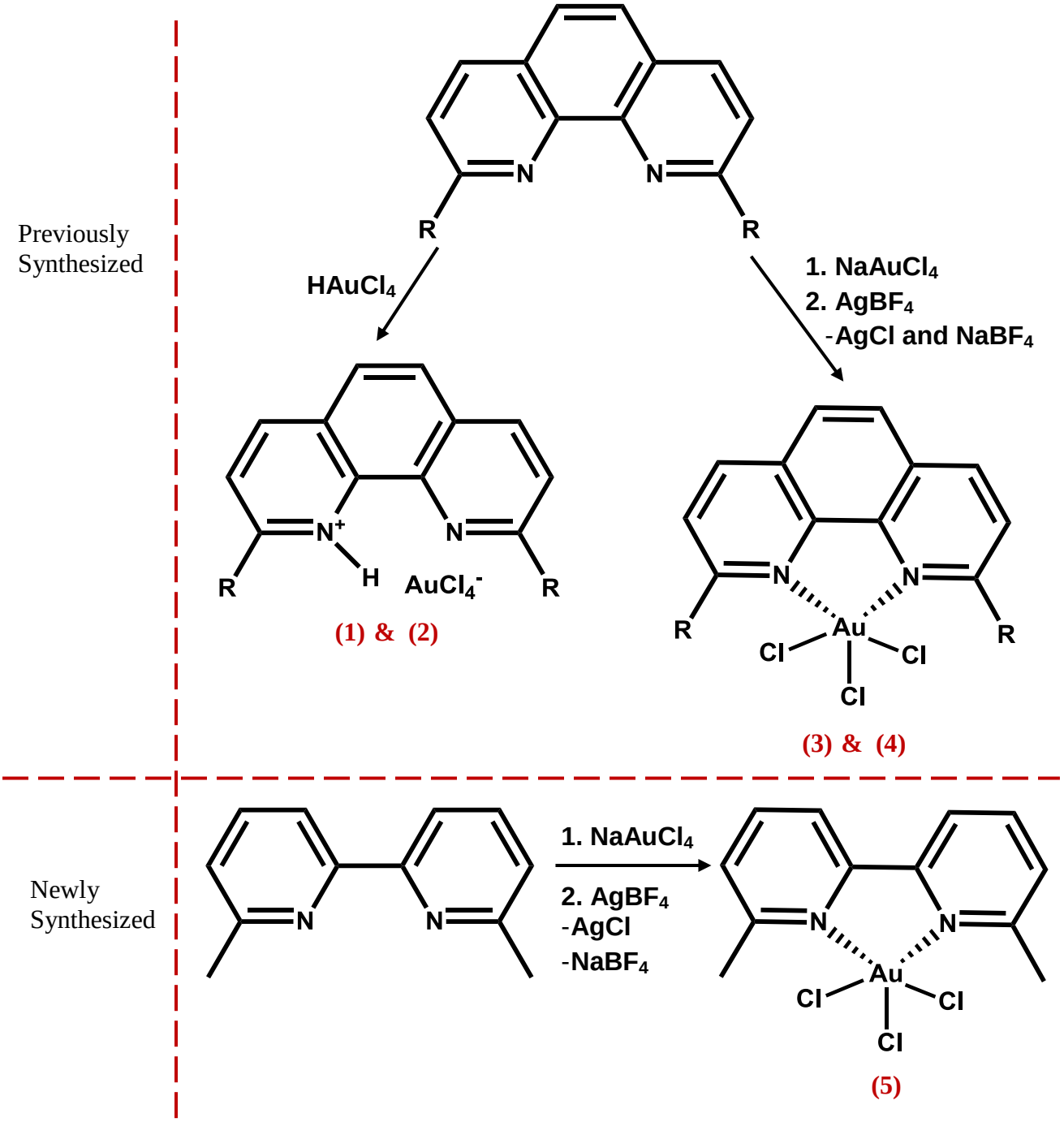

Scheme 1. Reaction schema for the syntheses of A) [^{R}phenH][$AuCl_4$] salts (R = *n*-butyl (**1**), *sec*-butyl (**2**)) and neutral distorted square pyramidal B) [(^{R}phen)$AuCl_3$] complexes (R = *n*-butyl (**3**), *sec*-butyl (**4**)) and C) the [(^{methyl}bipy)$AuCl_3$] complex (**5**).

Experimental:

General

[(^{R}phen)$AuCl_3$] and [^{R}phenH][$AuCl_4$] were synthesized previously as described in Scheme 1A and 1B, respectively.[24] $NaAuCl_4 \cdot 2H_2O$, $AgBF_4$, and ^{methyl}bipy were purchased from Sigma Aldrich. The solvents were used as purchased, without any further purification. Aside from eliminating exposure to direct sunlight, no specific handling measures were taken with the gold(III) complexes. The ^{1}H-NMR spectrum of **5** was recorded on a Varian Mercury 400 MHz spectrometer at 20°C; chemical shifts were referenced to residual solvent peaks. The infrared spectrum was recorded on a Varian Scimitar 800 Series FT-IR spectrophotometer with the use of KBr pellets, the UV-visible spectrum was recorded on a Cary 50 UV-Vis spectrophotometer and the CD spectra were recorded with a Jasco J-810 spectropolarimeter using 1.0 cm quartz cuvettes, and the elemental analyses were carried out by Atlantic Microlab Inc., Norcross, GA.

*Synthesis of [(^{methyl}bipy)$AuCl_3$] (**5**)*

[(^{methyl}bipy)$AuCl_3$] was synthesized in an analogous fashion to compounds **3** and **4** as previously described.[24] $NaAuCl_4 \cdot 2H_2O$ (0.685 g, 1.63 mmol) and ^{methyl}bipy ((0.3174 g, 1.63 mmol) were dissolved in 50 mL acetonitrile. This yellow reaction mixture was refluxed for 1 hour, followed by the addition of $AgBF_4$ (0.3003 g, 1.63 mmol). This solution was refluxed overnight, upon which an orange color formed, and the AgCl precipitate was filtered through a celite pad. The solvent was removed by rotary evaporation, the solid dissolved in methylene chloride (approximately 15 mL), and the resulting solution extracted with methylene chloride:deionized water (approximately 15 mL). The organic layer was isolated, dried with $MgSO_4$, filtered through celite, and removed *in vacuo* to yield a red/orange paste.

The solid was dissolved in a minimum of warm methylene chloride and orange needles formed overnight at 5°C. Elemental analysis: C = 29.66% and H = 2.43% (calculated: C = 29.56% and H = 2.48%.). UV-Visible spectroscopy: $\lambda_{max}(^{i}EtOH/CH_3CN, 20°C)/nm$ (ε, $M^{-1}•cm^{-1}$) = 225 (39, 100), 305 (17, 500), and 315-330 (broad shoulder). IR: ν_{max}/cm^{-1} = 3096 (CH), 2959, 2918, 2851 (CH), 1589, 1572 (conj. CC). ^{1}H NMR (300 MHz, $CDCl_3$, 20°C): δ 7.93 - 7.89 (m, 4H, H-3-6), 7.51 (d, 2H, H-2,7), and 3.14 (s, 6H, H-1,8) (See Scheme 2).

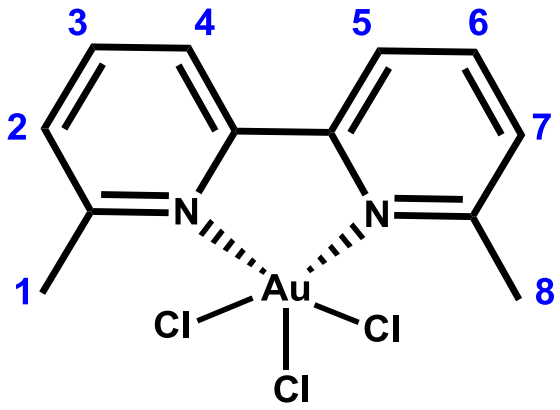

Scheme 2. Numbering scheme for compound 1 for ^{1}H NMR.

X-Ray Studies

For X-ray crystallography, suitable crystals of [(^{methyl}bipy)$AuCl_3$] were coated with Paratone N oil, suspended in a small fiber loop and placed in a cooled nitrogen gas stream at 173 K on a Bruker D8 APEX II CCD sealed tube diffractometer with graphite monochromated CuK_α (1.54178 Å) radiation. Data were measured using a series of combinations of phi and omega scans with 10 s frame exposures and 0.5° frame widths. Data collection, indexing and initial cell refinements were all carried out using APEX II software.[26] Frame integration and final cell refinements were done using SAINT software.[26] The structure was solved using Direct methods and difference Fourier techniques (SHELXTL, V6.12).[27] Hydrogen atoms were placed in their

expected chemical positions using the HFIX command and were included in the final cycles of least squares with isotropic U_{ij}'s related to the atom's ridden upon. All non-hydrogen atoms were refined anisotropically. Scattering factors and anomalous dispersion corrections are taken from the *International Tables for X-ray Crystallography*. Structure solution, refinement, graphics and generation of publication materials were performed by using SHELXTL, V6.12 software.

Stability Experiments

A 5 x 10^{-3} M stock solution of compound **5** was prepared by dissolving a 0.010 g sample of **5** in 4.00 mL of acetonitrile. A 7.0 µL aliquot of the gold complex stock solution was diluted in phosphate buffer to a final volume of 4 mL, yielding a gold(III) concentration of 1 x 10^{-5} M. A 4 mL solution of the 1 x 10^{-5} M gold(III) complex in 0.1 M phosphate buffer (pH 7.4) was prepared. UV-visible spectra of **5** was collected overnight at 20°C. These stability data were compared with previous experiments on compounds **1** and **4**.[24]

FT-IR spectra of the precipitate formed when a 5 x 10^{-4} M aqueous solution of the gold(III) complex (**5**) was stirred overnight at room temperature. The resulting precipitate was isolated from water and washed with diethyl ether (3 times). The remaining solid was dissolved in chloroform, and this solution was dried with $MgSO_4$ and filtered. This solution was analyzed by FT-IR spectroscopy.

Stability Experiments in the Presence of Biological Reductants

A 5 x 10^{-3} M stock solution of the gold complex was prepared by dissolving a 0.010 g sample of **5** was in 4.00 mL of acetonitrile. A 5 x 10^{-3} M ascorbic acid or glutathione stock solution was prepared by dissolving ascorbic acid or glutathione in phosphate buffer. A 7.0 µL

aliquot of the gold complex stock solution was added to 8 µL of the ascorbic acid/12 µL of the glutathione stock solution and diluted in 0.1 M phosphate buffer (7.4 pH) to a final volume of 4 mL, yielding a gold concentration of 1 x 10^{-5} M and a 1:1 ratio of gold complex to ascorbic acid or glutathione. UV-visible spectra of compound **5** were collected every hour over a 20 – 24 hour period (see Figures 5 and 6). These stability experiments were also carried out for compounds **1** and **4**.

DNA Binding- Ultrafiltration Experiments

A 0.010g sample of calf thymus DNA (ct-DNA) was dissolved in 10 mL of 10 mM phosphate pH 7.4 buffer (1 mM NaCl), resulting in a 1.5 x 10^{-3} M stock solution. The concentration of gold complex was 1 x 10^{-5} M and the ratio of complex/ct-DNA was r = 0.1 (that is, 10 base pairs DNA per molecule of the gold(III) complex) for compounds **1, 4,** and **5**. After incubating the gold complex-ct DNA mixture in buffer at 37°C (24 hrs for **5**; 30 minutes for **1** and **4**, the solution was passed through a 10,000 MW cutoff centrifugal filter (Amicon Ultra centrifugal filter units). Approximately 3 mL were collected in the lower portion and 1 mL was collected in the upper portion. The upper portion was diluted to 4 mL with phosphate buffer. Analysis of both portions was carried out via UV-visible spectroscopy by observing the presence/absence of the gold(III) chromophore at 320-400 nm.

DNA Binding – Circular Dichroism

A 0.010g sample of calf thymus DNA (ct-DNA) was dissolved in 10 mL of 10 mM phosphate pH 7.4 buffer (1 mM NaCl), resulting in a 1.5 x 10^{-3} M stock solution. The concentration of gold complex was 1 x 10^{-5} M and the ratio of complex/ct-DNA was r = 0.1 for

compound **5**. After incubation at room temperature for one hour, CD spectra were recorded of two DNA solutions, one with the gold(III) complex and one without the gold(III) complex.

Cellular Cytotoxicity Tests

Sulforhodamine B (SRB) cytotoxicity assays were utilized as described by Skehan *et. al.*[28] Descriptions of the tumor cell lines assessed can be found in Table 1. Cells were seeded in 96-well plates at a density of 4,000 cells/well overnight. Subsequently, the drugs were added (with concentrations ranging from 0–25 µM). This was followed by incubation at 37°C in 5% CO_2 conditions for 72 hours. These cells were then fixed for 1 hour with 10% cold trichloroacetic acid, followed by washing with water. Then, the plates were air-dried and stained with 0.4% SRB for 10 min. Furthermore, the plates were washed with 1% acetic acid and air-dried. The bound SRB was dissolved in 10 mM unbuffered Tris base (pH 10.5) and the plates were read with a microplate reader by detecting the absorbance of the sample at 492 nm. The percent survival was then calculated based upon the absorbance values relative to untreated samples. The experiment was repeated two times.

Table 1. Description of tumor cell lines utilized for this study.

Tumor Cell Line	Disease	Source	Species
H1703	Carcinoma	Lung	Human
A549	Non-small cell lung cancer, adenocarcinoma	Lung	Human
Tu212	Hypopharyngeal tumor	Head and Neck	Human
Tu686	Primary tongue cancer	Head and Neck	Human
886LN	Lymph node metastasis of squamous cell carcinoma	Head and Neck	Human

Western Blot Analysis

In order to determine in the mechanism of grown inhibition of the ^{secbutyl}phen ligand and compound **4**, western blots were carried out. Proteins from A549 cells treated with the ^{secbutyl}phen ligand and complex **4** were isolated and separated on a 10% SDS – polyacrylamide gel and then, transferred onto a polyvinylidene difluoride membrane. The membranes were blotted with primary antibodies against PARP, p21, and LC-3 and then, with the corresponding secondary antibodies. The signals were detected via an Amersham ECL (enhanced chemiluminescence) system by exposing each membrane to 2 mL of the ECL solutions for two minutes. A film of the membrane was developed in a darkroom in order to detect the protein expressions. This assay was repeated two times.

Results and Discussion:

Synthesis and Spectroscopic Characterization of [(^{methyl}bipy)$AuCl_3$]

Since [(2,9-dimethylphen)$AuCl_3$] (DMP-gold) was the only previously reported gold(III) complex possessing a 2,9-disubstituted phen ligand, we desired to prepare analogous gold(III) phen complexes bearing bulkier alkyl substituents.[24] However, we found that the use of auric acid ($HAuCl_4$) to synthesize ^{R}phen gold (III) complexes (R = *sec*-butyl, *n*-butyl) actually yielded salts comprised of protonated phen cations ($[phenH]^+$) and $[AuCl_4]^-$ anions, and not coordination complexes. Therefore, in an effort to promote direct coordination of the substituted phenanthroline, an alternative synthetic route was developed involving the reaction of $NaAuCl_4$ with ^{R}phen ligands, in the presence of silver(I) salts. This reaction resulted in the formation of one equivalent of AgCl and a neutral, distorted square pyramidal ^{R}phen gold(III) trichloride coordination complex. Initially, it was thought that the reaction with $HAuCl_4$ yielded direct

coordination of the ligand on the gold(III) metal center due to the fact that the UV-vis and ^{1}H NMR spectroscopic data for the [^{R}PhenH][$AuCl_4$] salts were similar to previous data reported for gold(III) coordination compounds possessing phen ligands. However, the X-ray crystal structures and elemental analyses for compounds **1** and **2** revealed the distinct difference between the coordination compounds and $AuCl_4^-$ salts.[24]

Since 6,6-dimethyl-2,2-bipyridine(^{methyl}bipy) is a commercially available ligand, we were able to synthesize the [(^{methy}bipy)$AuCl_3$] coordination compound in an analogous fashion to the previously reported [(^{R}phen)$AuCl_3$] complexes. The synthesis of compound **5** was successful, and high yields of orange crystalline needles can be readily obtained from dichloromethane. The ^{1}H NMR of compound **5** indicates that the ligand is coordinated to the gold(III) center, evidenced by the downfield shift of the methyl protons (from 2.61 to 3.14 ppm) and a distinct shift of the aromatic protons (two of the aromatic peaks shifted downfield by approximately 0.4 and 0.3 ppm, and the remaining aromatic peak shifted upfield by approximately 0.2 ppm; see Figure 4A and B). The UV-vis absorption spectrum of **5** corroborates the ^{methyl}bipy ligand coordination, confirmed by the presence of the ligand-to-metal charge transfer (LMCT) absorption (broad shoulder from 315-330 nm) and distinct shifts in the intraligand absorption maxima (Figure 5).

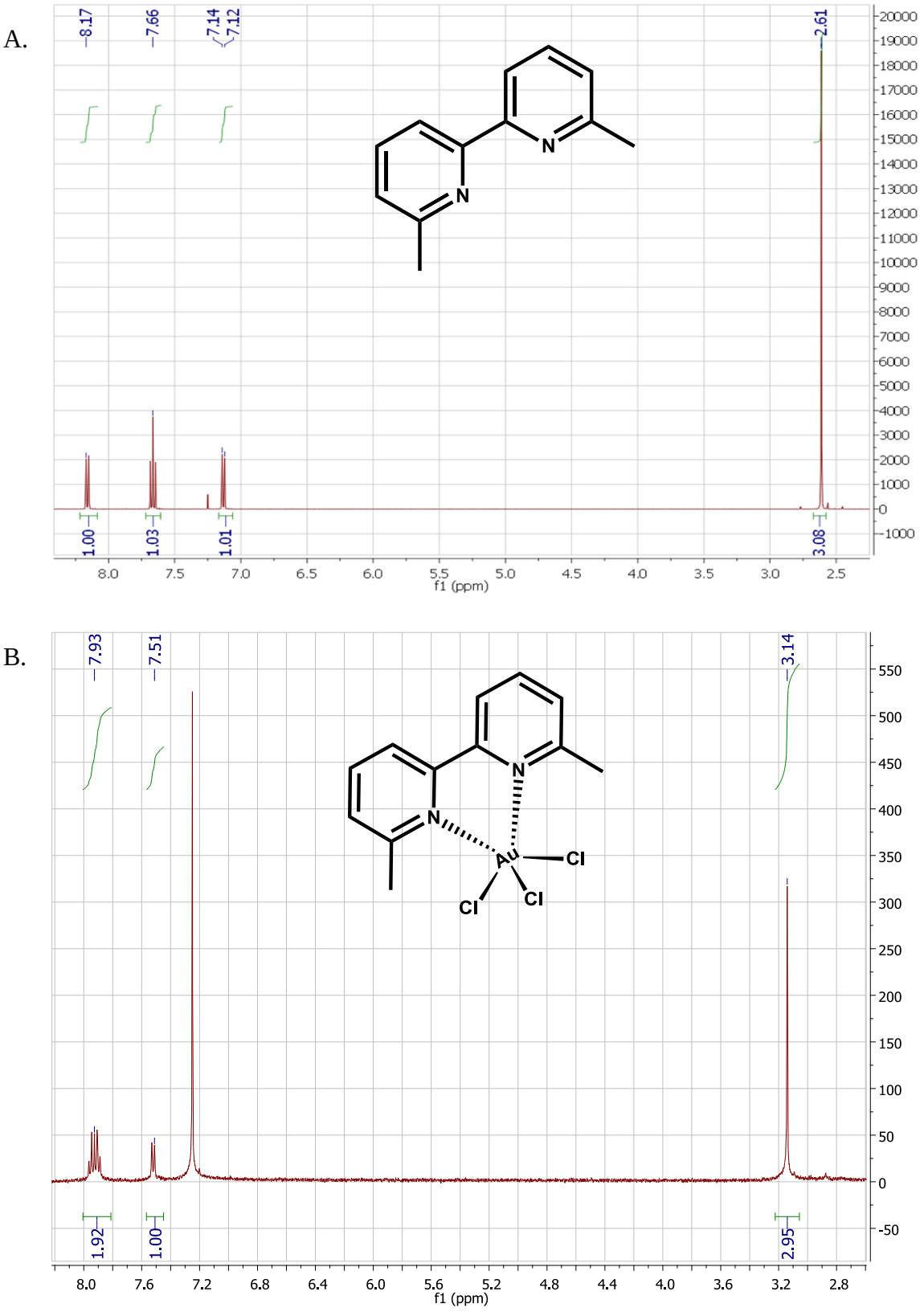

Figure 4. ^{1}H NMR spectra of A. the free ^{methyl}bipy ligand and B. [(^{methyl}bipy)$AuCl_3$]. (Both spectra were run in $CDCl_3$ solvent at 20ºC).

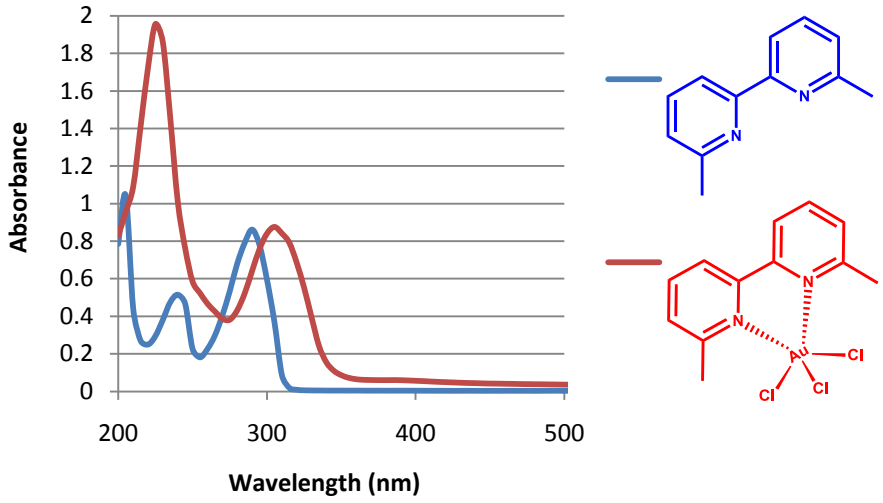

Figure 5. UV-vis spectrum of ^{methyl}bipy ligand (blue line) and [(^{methyl}Bipy)$AuCl_3$] (red line). (Both compounds were dissolved in a 2:1 ethanol/acetonitrile solvent mixture at a concentration of 5.0 x 10^{-5} M; the spectrum was collected at 20ºC)

X-Ray Crystal Structure of [(^{methy}bipy)$AuCl_3$]

Given our previous finding that the spectroscopic data is not definitive in determining the direct coordination of polypyridyl ligands,[24] we sought to characterize compound **5** via single crystal X-ray diffraction. The structural analysis of **5** provided unequivocal evidence that the ^{methyl}bipy ligand is directly coordinated to the gold(III) cation, and that the complex forms a distorted square pyramidal geometry (see Figure 6). Compound **5** is analogous to the previously reported [(^{R}phen)$AuCl_3$] complexes (compounds **3** and **4**)[24] and DMP-gold.[23] As reported for compounds **3**, **4**, and DMP-gold, the distorted square pyramidal geometry is also assigned to compound **5** based on the fact that the angles of the three chloride ligands and one nitrogen donor atom in the square pyramid base approach 90° (range of bond angles = 87.37°– 91.94°), and the other nitrogen donor atom from the ^{methyl}bipy ligand occupies the axial coordination position. The $Au–N_{axial}$ interatomic distance is elongated ($Au–N_{axial}$ =2.612 Å, $Au–N_{equatorial}$ =2.067 Å), and possesses a "lean" which accounts for the distortion of the square pyramid

(N_{axial}–Au–Cl = 113.16°, N_{axial}–Au–$N_{equatorial}$ = 71.8°). These structural features are comparable to those previously observed for compound **3**[24] and DMP-gold[23] (Au–N_{axial} =2.594 Å, Au–$N_{equatorial}$ =2.066 Å (**3**), Au–N_{axial} =2.584 Å, Au–$N_{equatorial}$ =2.09 Å (DMP-Gold); N_{axial}–Au–Cl = 109.1°, N_{axial}–Au–$N_{equatorial}$ = 73.2°(**3**), N_{axial}–Au–Cl = 111.1°, N_{axial}–Au–$N_{equatorial}$ = 73.4°(DMP-gold)).

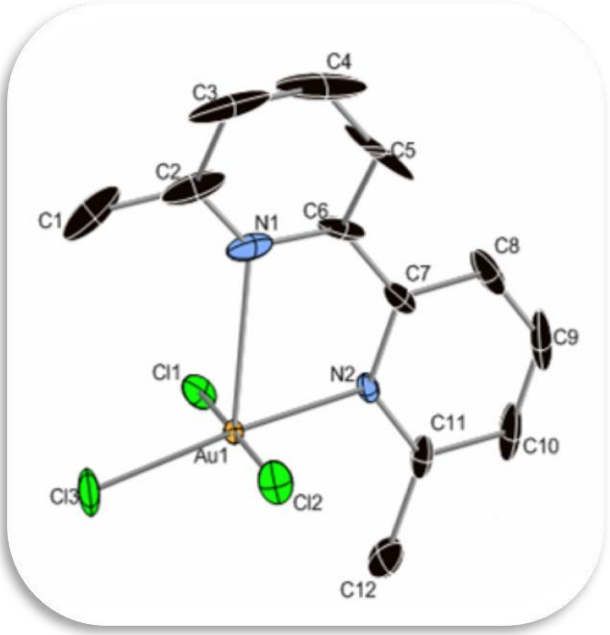

Figure 6. Thermal ellipsoid plot of the crystal structure for [(^{methyl}bipy)$AuCl_3$] (**5**) drawn at 50% probability; hydrogen atoms have been omitted for clarity. Selected bond lengths in Å are as follows: Au–N(2) 2.067(5), Au–N(1) 2.612(6), Au–Cl(3) 2.2690(19), Au–Cl(2) 2.280(2), and Au–Cl(1) 2.2810(19). Selected angles in ° are as follows: N(2)–Au–Cl(3) 174.84(16), N(2)–Au–Cl(2) 90.79(14), Cl(3)–Au–Cl(2) 90.24(7), N(2)–Au–N(1) 71.8(2), and Cl(3)–Au–N(1) 113.16(18).

Table 2. Crystal and refinement data for compound **5.**

Empirical formula	$C_{12}H_{12}AuCl_3N_2$
Formula weight	487.55
Temperature (K)	173(2)
Wavelength (Å)	0.71073
Crystal System	Monoclinic
Space Group	$P2_{(1)}/c$
V (Å^3)	1441.2(12)
Z	4
a (Å)	7.740(4)
b (Å)	9.821(5)
c (Å)	19.038(9)
α(°)	90.
β(°)	95.233(7)
γ(°)	90.
Density (calculated) (Mg/m^3)	2.247
Reflections collected	21071
Independent reflections	4173 [R(int) = 0.0396]
Max. and min. transmissions	0.6156 and 0.1466
Final R indices [*I>2σ(I)*]	R1 = 0.0381, wR2 = 0.0955
R indices (all data)	R1 = 0.0420, wR2 = 0.0984
Goodness of Fit	1.072

Stability Studies

The stability of compounds **1**-**4** in physiological buffer was previously reported.[24] These experiments suggested the formation of a hydroxo species in solution, [(^{R}phen)Au(OH)$_x$(Cl)$_y$] or [^{R}phenH][Au(OH)$_x$Cl$_y$], and a decrease in solubility of both the [^{R}PhenH][AuCl$_4$] salts and [(^{R}Phen)AuCl$_3$] complexes.[24] The stability of the [(^{methyl}bipy)AuCl$_3$] complex in physiological buffer has also been carried out (Figure 7). It is noted that compound **5** did not exhibit a significant change in UV-vis absorption overnight, nor the formation of any precipitate,

indicating this complex is more soluble than compounds **1**-**4** in aqueous buffer; the increased solubility of **5** in buffer is possibly due to the decreased hydrocarbon character of the ligand. The formation of a hydroxo complex ([(^{methyl}bipy)Au$(OH)_x(Cl)_y$]) was observed however at higher concentrations (Scheme 3), as the isolated precipitate possessed an –OH stretch at 3425 cm^{-1} in the FT-IR spectrum. Similar to compounds **3** and **4**, -C=C-H stretches at 3019 cm^{-1}, and -C=C stretches at 1521 cm^{-1} and 1655 cm^{-1} were detected in the FT-IR spectrum of the precipitate, indicating that the ^{methyl}bipy ligand is still coordinated to gold(III) metal center. Although the Au(III)-Cl bonds are labile in solution, the spectroscopic evidence suggests that the polypyridyl ligands remain coordinated to the gold(III) center, indicating that the polypyridyl ligand design is most likely retained in a physiological environment.

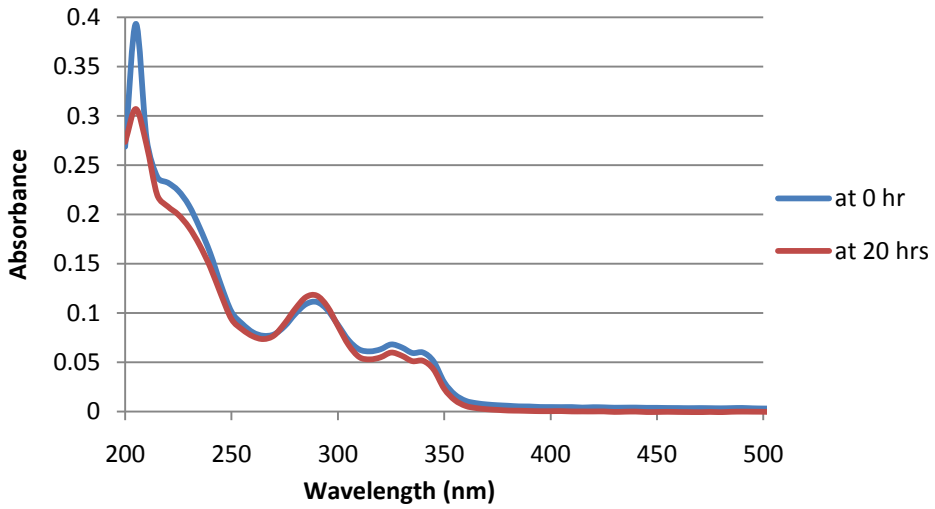

Figure 7. UV-vis spectrum of **5** in pH 7.4 phosphate buffer over a 20 hour period; 1.0 x 10^{-5} M gold complex; the spectrum was collected at 20°C.

$$[(^{methyl}bipy)AuCl_3(aq) + xH_2O(l) \rightleftharpoons [(^{methyl}bipy)Au(H_2O)_x(Cl)_y](aq) + (3\text{-}y)Cl^-(aq)$$

$$[(^{methyl}bipy)Au(H_2O)_x(Cl)_y](aq) \rightleftharpoons [(^{methyl}bipy)Au(OH)_x(Cl)_y](aq) + xH^+(aq)$$

Scheme 3. Proposed mechanism of formation of gold(III) hydroxo precipitate.

The stability of **1, 4,** and **5** has also been compared upon exposure to the biological reductants reduced glutathione (GSH) and ascorbic acid. The complexes (compounds **4** and **5**) and the salt (compound **1**) both exhibit a decrease in absorbance over time in the UV-vis spectrum upon the addition of glutathione (Figure 8). The spectra for **1** and **4** look similar to those obtained from the stability studies conducted in plain buffer, indicating the GSH does not have a significant effect on their stability. However, compound **5** undergoes a significant decrease in absorbance, suggesting that its solubility decreases upon the addition of GSH to the solution. Since the intraligand absorption maximum does not appear to shift and no formation of colloidal gold(0) is observed, it is likely that reduction of **5** is not occurring. Upon exposure to ascorbic acid, compounds **1**, **4**, and **5** all experience a decrease in absorption at 320 nm and form a new absorption maximum at 550-600 nm, indicative of the formation of elemental gold (Figure 9). However, the coordination complexes **4** and **5** appear to display reduction at a slower rate than the [^{R}phenH][$AuCl_4$] salt (**1**), as observed by the less rapid decrease in the gold absorption at 320 nm. This is likely due to the fact that direct coordination of the ^{R}phen and ^{methyl}bipy ligands stabilizes the gold(III) center, and the unbound $[AuCl_4]^-$ anion in **1** is more susceptible to the biological reductant.

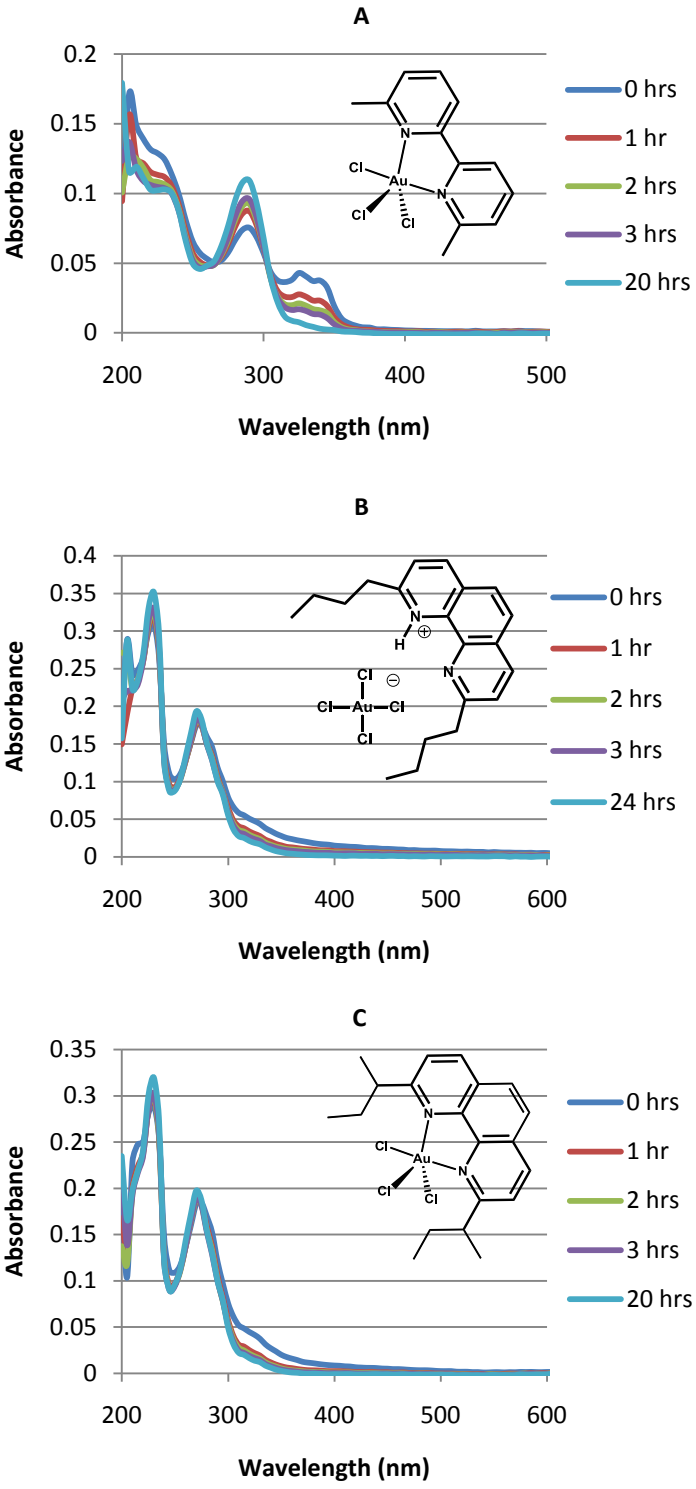

Figure 8. UV-visible absorption spectra of A) **5** B) **1**, and C) **4** in a glutathione/pH 7.4 phosphate buffer solution (1 x 10^{-5} M glutathione and gold complex; 20 °C).

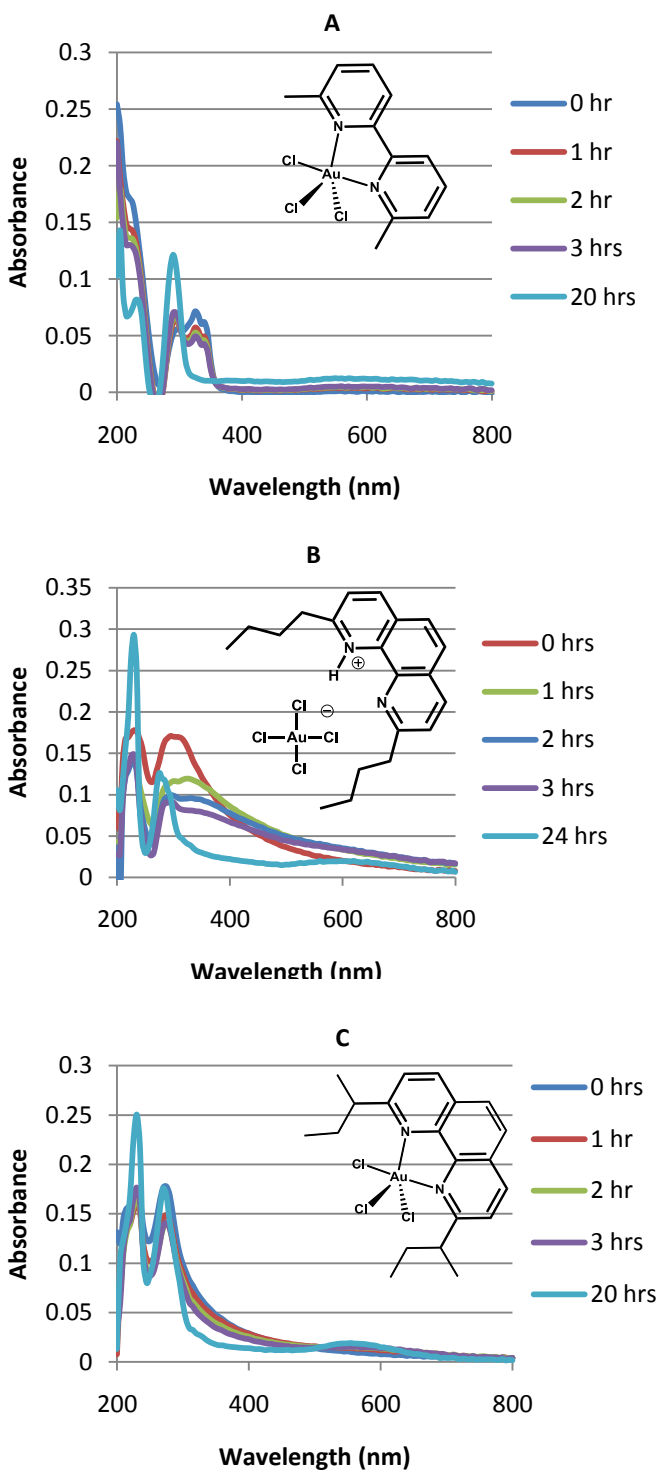

Figure 9. UV-visible absorption spectra of A) **5** B) **1** and C) **4** in an ascorbic acid/pH 7.4 phosphate buffer solution (1 x 10^{-5} M ascorbic acid and gold complex; 20 °C).

DNA Binding Studies

As previously stated, even though studies have found that gold(III) coordination compounds have the ability to interact with DNA, the strength of this interaction is often variable and of lower affinity than *cis*-platin.[8] This is highly advantageous since a different mechanism of cytotoxicity provides the potential to target cancer cell lines that are resistant to platinum-based therapies and to assuage some of the mutagenic side effects associated with *cis*-platin. The interactions between the transition metal complexes and DNA can occur via two main mechanisms: 1) electrostatic interactions or 2) intercalation. Electrostatic interactions usually occur between the metal center and the negatively charged phosphate backbone while intercalation occurs via $\pi - \pi$ stacking of the aromatic ligand and the DNA base pairs (Figure 10).[29]

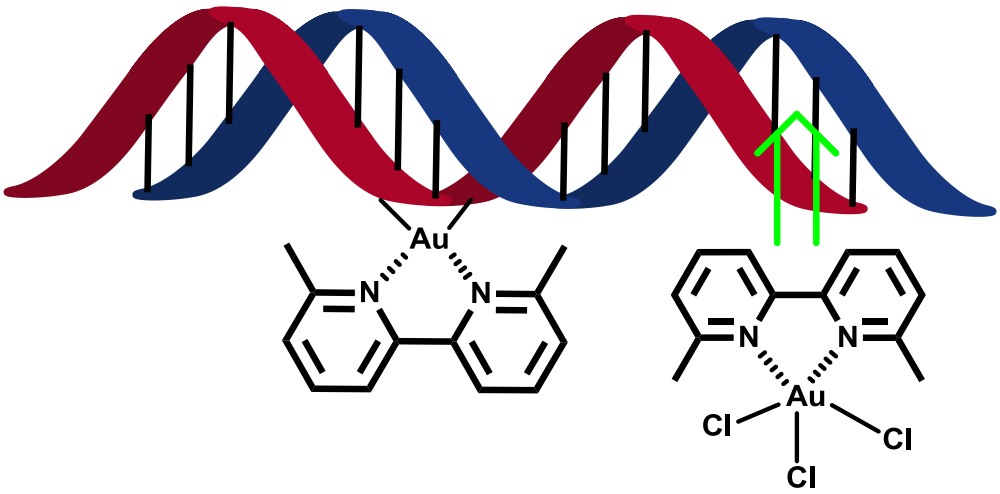

Figure 10. Two possible DNA binding interactions between **5**: electrostatic interactions (left) and intercalation (right).

In an attempt to obtain qualitative DNA binding data, ultrafiltration experiments were carried out (Figure 11). The results from this experiment indicate that compound **5** has the ability to bind to DNA but that this binding is incomplete. This partial DNA binding is demonstrated by the fact the (+) DNA trial possessed free gold complex in the flow-through, though at a lower concentration than observed for the (-) DNA control experiment (see Figure 11B), and by the fact that the upper portion of the (+) DNA trial displayed a stronger gold absorption than the upper portion of (-) DNA control (see Figure 11A).

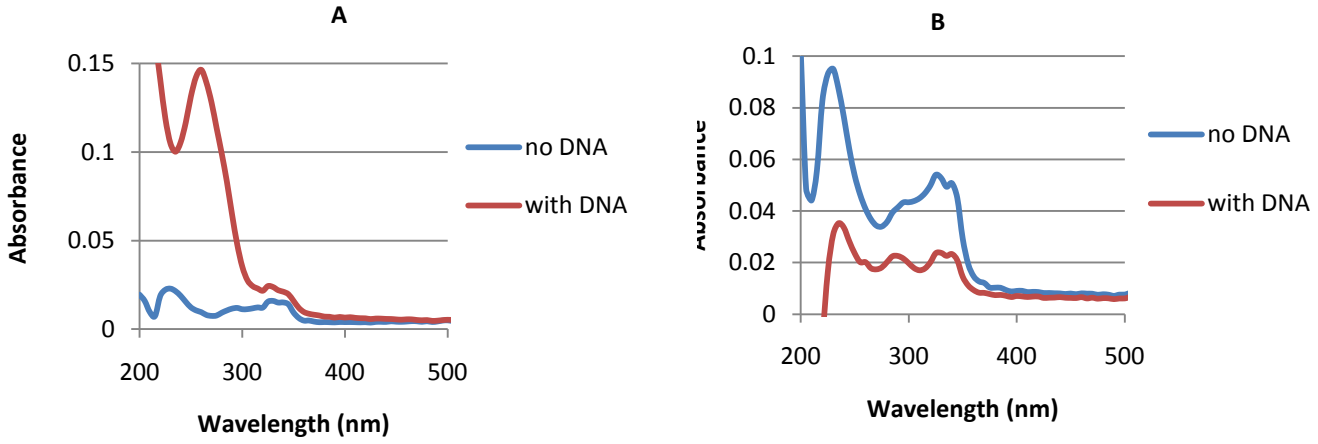

Figure 11. UV-Visible spectra of compound **5** with and without calf thymus DNA in pH 7.4 phosphate buffer (1 x 10^{-5} M gold complex; 10 base pairs DNA per gold atom; 37°C). Samples were passed through a 10 kDA MW cutoff filter; A) top layer remaining after filtration; B) flow-through after filtration.

These results are supported by the CD spectra obtained (Figure 12). While through UV-visible spectroscopy, the effect of DNA binding on the gold(III) chromophore can be monitored, CD spectra reveal changes in DNA conformation by ligand binding.[12] The CD spectra of the DNA includes a positive band at 275 nm, correlating to base-stacking, and a negative band at 245 nm, correlating to the right-hand conformation of the helix.[30] From these spectra, a redshift of the positive band by about 3 nm is discernable while no significant shift is observed for the

negative band. This suggests that complex **5** might have a more prominent effect of the base-stacking of the DNA rather than its helical nature; this is supported by previous findings reported by Shi et. al.[29] Significant decreases in the CD signal indicate that **5** induced changes in the DNA conformation and may intercalate with DNA. However, minimal shifts in the bands imply that the **5**-DNA intercalation may not be very strong.

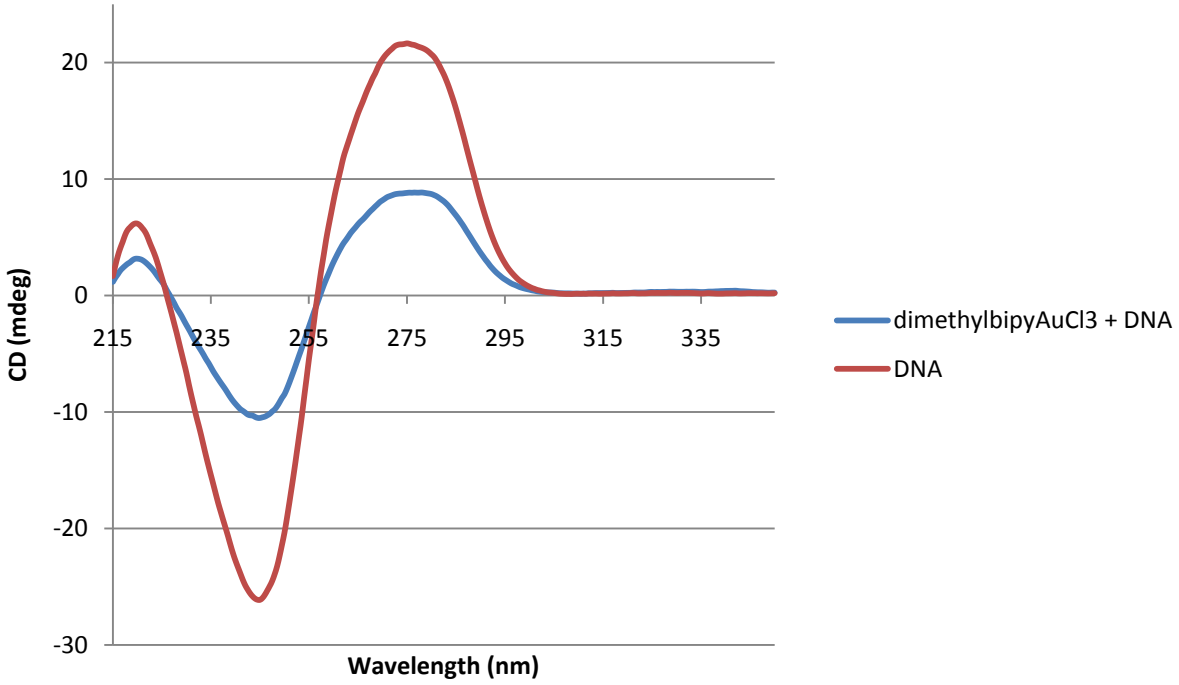

Figure 12. CD spectrum of compound **5** with and without calf thymus DNA in pH 7.4 phosphate buffer (1 x 10^{-5} M gold complex; 10 base pairs DNA per gold atom; room temperature).

It is noted that due to the more limited solubility for compounds **1** and **4**, DNA binding studies could not be completed. Changes in λ_{max} at 320 nm were observed, but since changes were also observed in the stability experiments with plain buffer, there was no trend in λ_{max} that could be solely associated with the addition of DNA. Additionally, distinct gold(III) absorption maxmima were not observed in the upper or lower fractions of the ultrafiltration studies, making conclusions about qualitative DNA binding difficult to make.

Cellular Cytotxicity

Testing of compounds **1**, **4**, and **5** for cytotoxicity against existing lung and head and neck cancer cell lines provided insight into the mechanism of cytotoxicity for gold(III) polypyridyl complexes (see Table 3, Figure 13). Foremost, it was found that compounds **1** and **4** exhibited significantly higher cytotoxicity than *cis*-platin against existing cancer cell lines, generally having IC_{50} values 2-8 times lower than *cis*-platin, and IC_{50} values as much as 80 times lower for compound **1** and 40 times lower for compound **4** (against the H1703 tumor cell line; Table 3). Compound **5** displayed considerably lower cytotoxicity; it was three times more potent than *cis*-platin against the H1703 line, but had greater IC_{50} values than *cis*-platin against all of the other tumor cell lines (see Table 2). Additionally, the free $^{sec\text{-butyl}}$phen ligand displayed the most potent cytotoxicity in cell line 886LN while the $AuCl_4^-$ salt possessed minimal cancer cell cytotoxicity in all of the cell lines.

Table 3. IC_{50} values for the gold(III) polypyridyl complexes, free $^{sec\text{-butyl}}$phen ligand, and *cis*-platin against tumor cell lines (A549, 886LN, Tu212, Tu686, H1703)

	A549 (μM)	**886LN (μM)**	**Tu212 (μM)**	**Tu686 (μM)**	**H1703 (μM)**
[(^{methyl}bipy)$AuCl_3$] (5)	4.36	23.3	12.8	N/A	2.4
[($^{sec\text{-butyl}}$phen)$AuCl_3$] (4)	0.76	1.6	0.34	1.16	0.2
$^{sec\text{-butyl}}$phen ligand (Control)	0.08	0.18	0.07	0.09	0.07
[$^{n\text{-butyl}}$phenH][$AuCl_4$] (1)	0.37	1.13	0.16	0.38	0.09
***Cis*-platin**	3.1	4.2	2.7	2.9	7.9

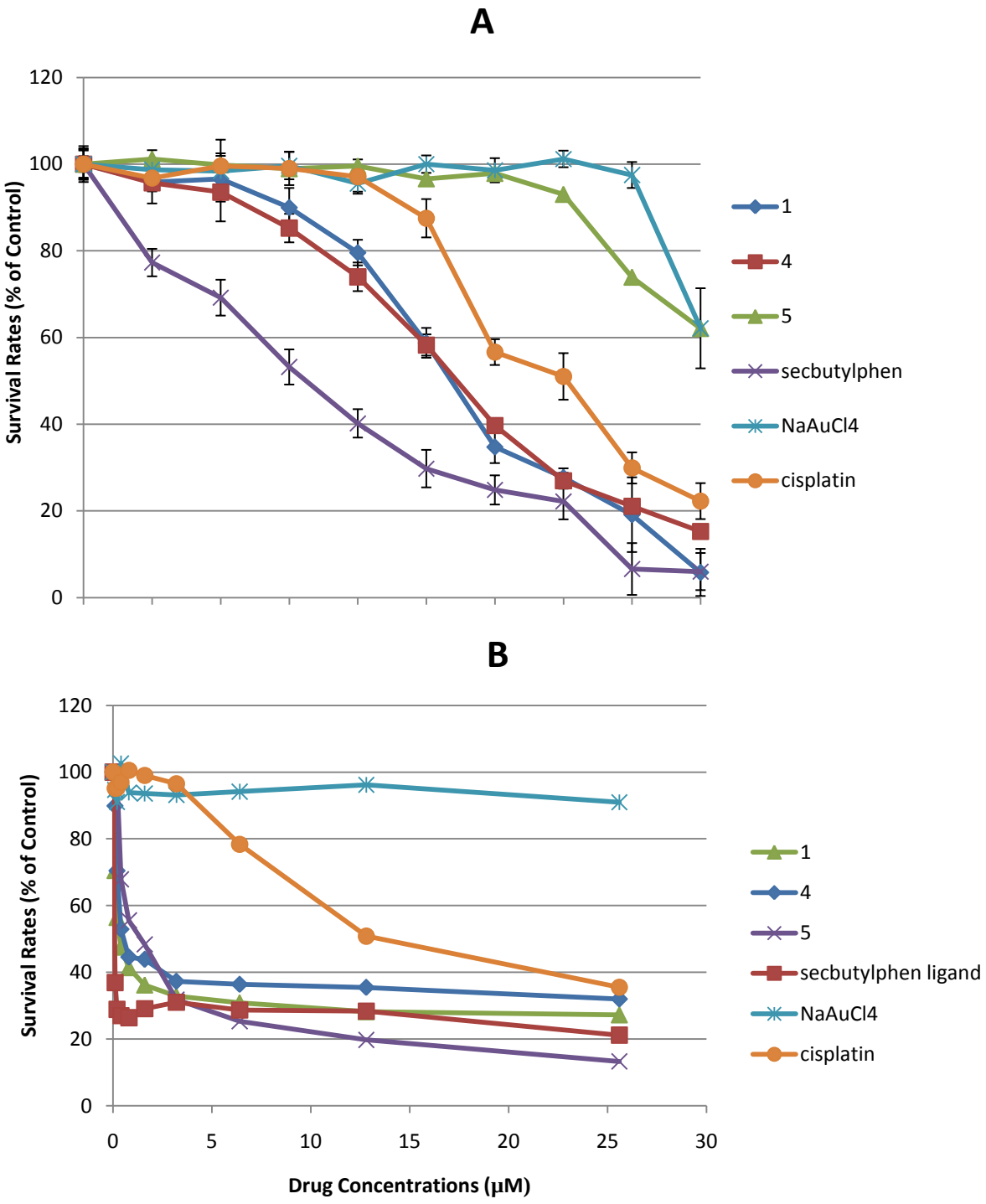

Figure 13. Representative cytotoxicity assay on cancer cell line: **A)** 886LN and **B)** H1703 [sulforhodamine B (SRB) cytotoxicity assay]. All of the experiments were repeated twice.

Cell Death Pathway/Cell Cycle Arrest

In order to learn more about the pathway that the cytotoxic *sec*-butylphen ligand and [(*sec*-butylphen)$AuCl_3$] complex utilize to induce their antiproliferative activity, A549 lung cancer cells were treated with varying concentrations of these therapeutics and the proteins from these cells were collected. Western blot assays assisted in detecting the expression of specific relevant proteins, which served as indicators for a specific cytotoxic mechanism, in the treated cells. That is, a reliable protein marker for apoptosis is poly(ADP-ribose) polymerase (PARP), for cell cycle arrest is p21 (specifically G_1 arrest), and for autophagy is microtubule-associated protein light chain 3 (LC3). As per normal cellular function, PARP assists with the repair of DNA strand breaks when DNA damage occurs. This process can deplete the cell's ATP storage and therefore, during apoptosis, PARP is often times cleaved to preserve the cellular energy source.[16] During autophagy, the LC3 protein is vital in propagating the degradation of cellular organelles and proteins when autophagosomes fuse with lysosomes.[31] p21 is a cyclin – dependent kinase inhibitor. During the normal cell cycle, cyclin – dependent kinases (CDK) act as regulatory proteins that are activated at certain points of the cell cycle to assist with transitioning from one phase to another. High expression of p21 inactivates an important G_1 cyclin-CDK complex and inhibits the cell from progressing onto the S (synthesis) phase.[32]

The Western Blot results for the ligand treatment showed increasing protein expression for cleaved PARP, p21, and LC-3 at increasing concentrations of the ligand (Figure 14A). Therefore, our results suggested that the action mechanism of the ligand involved apoptosis induction, cell cycle arrest, and cell autophagy. Treatment with **4** revealed very unique results that were significantly different than those of ligand treatment (Figure 14B). As expected, consistent expression of full PARP was seen in the control and treated A549 cells. However, at 4

μM treatment of **4**, a second band (referring to PARP cleavage) was expressed, suggesting strong apoptotic induction. Expression of p21 was highest at the low drug concentration of 0.5 μM but seemed to decrease at higher concentrations. The p21 expression in the control could be due to high confluence of the treated cells but, since the confluency was consistent for each treatment, we can focus on the changes in p21 expression. LC3 expression increased until a concentration of 1 μM of the drug but was significantly lower at the highest concentration. These outcomes suggest that at high concentrations of **4**, most of the cells undergo apoptosis induction, which implies that fewer cells are subject to cell cycle arrest and autophagy. On the other hand, at very low drug concentrations, cells undergo cell cycle arrest and at intermediate concentrations, autophagy-induced cell death occurs. This shows a progression of A549 cell antiproliferative mechanism from cell cycle arrest to autophagy to apoptosis with increasing concentrations of **4**. It is important to point out that cell treatment with the $^{sec\text{-butyl}}$phen ligand and **4** were carried out because they exhibited significant cytotoxicity while complex **5** had much lower anti-cancer potency.

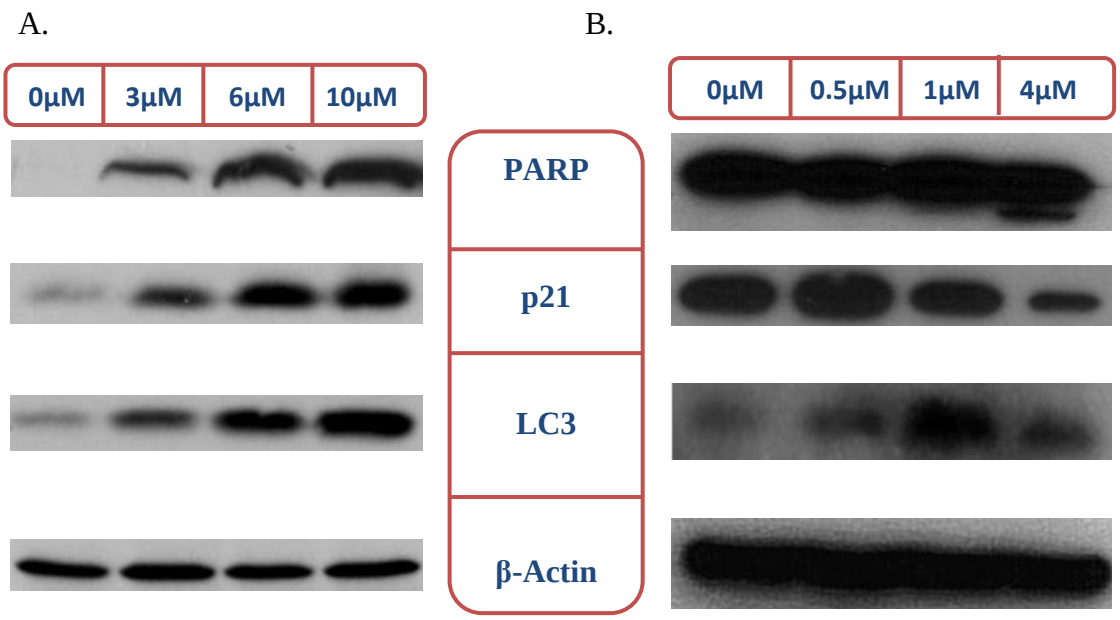

Figure 14. Western Blot assays for A. *sec*-butylphen ligand treatment (concentrations = 0, 3, 6, and 10 μM) of A549 cells for 24 hours and B. [(*sec*-butylphen)$AuCl_3$] (**4**) treatment (concentrations = 0, 0.5, 1, 4 μM) of A549 cells for 48 hours. Note: β-actin was used as a loading control. Also, for treatment with the ligand, only the cleaved PARP expression is shown whereas for treatment with **4**, the top bands correspond to PARP and the bottom bands correspond to cleaved PARP.

Conclusion:

Gold coordination compounds represent a growing class of potential anti-cancer therapeutics. Therefore, it is important to gain more insight into how gold-based therapeutics impart tumor cell cytoxicity and begin to correlate the *in vitro* behavior of these compounds to their therapeutic effects. DNA binding and stability studies of compounds **1**, **4**, and **5** indicate that these gold(III) complexes do not undergo complete DNA binding, and that direct coordination of the polypyridyl ligand and bulky side chains may provide protection for the gold(III) center against biological reductants such as glutathione and ascorbic acid. *In vitro* cytotoxicity assays reveal that complexes **1** and **4** are more potent than *cis*-platin against existing cancer cell lines. Also, it is important to note that the *sec*-butylphen ligand possesses the highest anti-cancer potential; this

finding is consistent with previous reports that show *in vitro* anti-cancer efficacy of 1,10-phenanthroline (phen) and 2,2′:6,2″-terpyridine (terpy) ligands comparable to or higher than the gold(III) complexes of these ligands.[9, 30] Therefore, this raises the possibility that the ligand is released in the cellular environment, implicating that the ligand could be the cytotoxic agent rather than the gold(III) complex. This is especially of concern since Messori et. al.[9] and Eichler et. al.[33] have provided evidence of ligand release in the presence of biological reductants with both the ligand and the gold(III) complex exhibiting substantial cytotoxicity. However, complex **4** does not seem to release the ligand in the presence of glutathione since no distinct shift of the phen-based intraligand absorption maximum and no gold(0) formation is observed. However, since these studies are performed in non-cellular environments, more insight into this mechanism in tumor cells is needed, which can be provided by the western blot assays.

Through analysis of protein expression, is has been ascertained that complex **4** induces cell cycle arrest at low concentrations, autophagy at intermediate concentrations, and apoptosis at high concentrations. Since it appears that compound **4** initiates its anti-proliferative activity differently than the free $^{sec\text{-butyl}}$phen ligand, this suggests that perhaps the ligand is not released and the gold complex acts as the cytotoxic agent. Still, to arrive at a more definitive conclusion, more experiments need to be carried out. These could include tagging the ligand with a fluorescent tag in order to monitor the ligand-gold complex in a cellular environment using microscopy or treating cell media not only with the drug (ligand or gold(III) complex) but also with other metal ions, which should inhibit the cytotoxic effects of the free ligand but not the gold complex.[34]

Furthermore, to fully understand the exact anti-cancer mechanism of these gold(III) compounds, the TrxR inhibition capabilities of these compounds needs to be investigated. DNA melting curves or titrations curves with CD can also provide us with more quantitative DNA

binding constants. Comparison of these two data sets will enable us to conclude which anti-cancer pathway is most prominent for these gold(III) therapeutics. Also, on-going research is seeking to explore the systemic toxicity of these complexes by performing *in vivo* tests on mice models.

References:

[1] Sundquist, W. I.; Lippard, S. J. *Coord. Chem. Rev.,* **1990**, *100*, 293.

[2] van Zutphen, S.; Reedijk, J. *Coord. Chem. Rev*., **2005**, *249*, 2845.

[3] Jamieson, E. R.; Lippard, S. J. *Chem. Rev.*, **1999**, 99, 2467-2498.

[4] Kelland, L.R. *Cisplatin: Chemistry and Biochemistry of a Leading Anticancer Drug*, ed. B. Lippert, Verlag Helvetica Chimica Acta, Zurich; Wiley-VCH, Weinheim, Germany, **1999**, 497-521.

[5] Agarwal, A.; Balla1, J.; Alam, J.; Croatt, A. J.; Nath, K. A. *Kidney International.*, **1995**, 48, 1298.

[6] Hamers, F.; Brakkee, J.; Cavalletti, M.; Marmonti, L.; Pezzoni, J.; Gispen, W. *Cancer Research.,* **1993**, 53, 544.

[7] Deegan, C.; Coyle, B.; McCann, M.; Devereux, M.; Egan, D.A. *Chemico-Biological Interactions,* **2006**, 164, 115.

[8] Tiekink, E. R. *Critical Reviews in Oncology/Hematolog*, **2002**, 42, 225.

[9] Messori, L.; Abbate, F.; Marcon, G.; Orioli, P.; Fontani, M.; Mini, E.; Mazzei, T.; Carotti, S.; O'Connell, T.; Zanello, P. *J. Med. Chem.*, **2000**, 43, 3541.

[10] Milacic, V. and Dou, Q.P. *Coord. Chem. Rev.*, **2009**, *253*, 1649.

[11] Fries, J. F.; Bloch, D.; Spitz, P.; Mitchell, D. M. *The Amer. J. of Med.*, **1985**, 78, 56.

[12] Messori, L.; Orioli, P.; Tempi, C.; Marcon, G. *Biochem. and Biophys. Research Comm.*, 2001, **281**, 352.

[13] Wang, D.; Lippard, S.J. *Nature Reviews Drug Discovery*, **2005**, 4, 307.

[14] Rigobello, M.P.; Messori, L.; Marcon, G.; Agostina Cinellu, M.; Bragadin, M.; Folda, A.; Scutari, G.; Bindoli, A. *J. Inorg. Biochem.,* **2004**, *98*, 1634.

[15] Tiekink, E.R.T. *Inflammopharmacol,* **2008**, 16, 138.

[16] Hotchkiss, R. S.; Strasser, A.; McDunn, J.E.; Swanson, P.E. *N. Engl. J. Med.* **2009**, 361, 1570.

[17] Ronconi, L.; Giovagnini, L.; Marzano, C.; Bettio, F.; Graziani, R.; Pilloni, G.; Fregona, D. *Inorg. Chem.*, **2005**, 44, 1867.

[18] Ronconi, L.; Marzano, C.; Zanello, P.; Corsini, M.; Miolo, G.; Macca, C.; Trevisan, A.; Fregona, D. *J. Med. Chem.*, **2006**, 49, 1648.

[19] Messori, L.; Marcon, G.; Orioli, P. *Bioinorg. Chem. Appl.*, **2003**, 1, 177.

[20] Heffeter, P.; Jakupec, M.A.; Korner, W.; Wild, S.; von Keyserlingk, N.G.; Elbling, L.; Zorbas, H.; Korynevska, A.; Knasmuller, S.; Sutterluty, H.; Micksche, M.; Keppler, B.K.; Berger, W. *Biochem Pharmacol*, **2006**, **71**, 426.

[21] Zhao, G.; Sun, H.; Lin, H.; Zhu, S.; Su, X.; Chen, Y. *J. Inorg. Biochem*., **1998**, 72, 173.

[22] Aguirre, J.D.; Angeles-Boza, A.M.; Chouai, A.; Turro,C.; Pellois, J.P.; Dunbar, K.R. *Dalton Trans*, **2009**, 28, 10806.

[23] Robinson, W.T. and Sin, E. *J. Chem. Soc., Dalton Trans*., **1975**, 726.

[24] Hudson, Z.D.; Sanghvi, C.D.; Rhine, M.A.; Ng, J.J.; Bunge, S.D.; Hardcastle, K.I.; Saadein, M.R.; MacBeth, C.E.; Eichler, J.F. *DaltonTrans.* **2009**, 7473.

[25] Pallenberg, A. J.; Koenig, K. S.; Barnhart, D. M. *Inorg. Chem*., **1995**, 34, 2833.

[26] Beltran, L.M.C.; Long, J. R. *Acc. Chem. Res.* **2005**, *38*, 325.

[27] Sheldrick, G.M. *Acta Crystallographica Section A.* **2008**,*64*, 112.

[28] Skehan, P.; Storeng, R.; Scudiero, D.; Monks, A.; McMahon, J.; Vistica, D.; Warren, J.T.; Bokesch, H.; Kenney, S.; Boyd, M.R. *J. Natl. Cancer Inst*. **1990**, 82, 1107–12.

[29] Kumar, C.V.; Barton, J.K.; Turro, N.J. *J. Am. Chem. Soc.*, **1985,** *107*, 5518-5523.

[30] Shi, P.; Jiang, Q.; Zhao, Y.; Zhang, Y.; Lin, J.; Lin, L.; Ding, J.; Guo, Z. *J. Biol. Inorg. Chem.*, **2006**, 11, 745.

[31] Tanida, I.; Ueno, T.; Kominami, E. *Methods Mol. Biol*., **2008**, 445, 77.

[32] Vermeulen, K.; Van Bockstaele, D.R.; Berneman, Z.N. *Cell Prolif.*, **2003**, 36, 131.

[33] Wein, A.N.; Stockhausen, A.T.; Harcastle, K.I.; Saadein, M. R.; Peng, S.; Wang, D.; Shin, D.M.; Zhuo, G.C.; Eichler, J.F. *J. Inorg. Biochem.*, **2011**, 105, 663.

[34] Torti, S.V.; Torti, F.M.; Whitman, S.P.; Brechbiel, M.W.; Park, G.; Planalp, R.P. *Blood*, **1998**, 92, 1384.

Appendix - Crystallographic Data for Complex 5:

Table 1. Crystal data and structure refinement for JFEIX_19.

Identification code	JFEIX_19	
Empirical formula	C12 H12 Au Cl3 N2	
Formula weight	487.55	
Temperature	173(2) K	
Wavelength	0.71073 Å	
Crystal system	Monoclinic	
Space group	P2(1)/c	
Unit cell dimensions	a = 7.740(4) Å	α= 90°.
	b = 9.821(5) Å	β= 95.233(7)°.
	c = 19.038(9) Å	γ = 90°.
Volume	1441.2(12) $Å^3$	
Z	4	
Density (calculated)	2.247 Mg/m^3	
Absorption coefficient	10.746 mm^{-1}	
F(000)	912	
Crystal size	0.29 x 0.15 x 0.05 mm^3	
Theta range for data collection	2.15 to 30.40°.	
Index ranges	-10<=h<=10, -13<=k<=13, -27<=l<=26	
Reflections collected	21071	
Independent reflections	4173 [R(int) = 0.0396]	

Completeness to theta = 30.40°	96.1 %
Absorption correction	Semi-empirical from equivalents
Max. and min. transmission	0.6156 and 0.1466
Refinement method	Full-matrix least-squares on F^2
Data / restraints / parameters	4173 / 0 / 105
Goodness-of-fit on F^2	1.072
Final R indices [I>2sigma(I)]	R1 = 0.0381, wR2 = 0.0955
R indices (all data)	R1 = 0.0420, wR2 = 0.0984
Largest diff. peak and hole	2.807 and -2.065 e.$Å^{-3}$

Table 2. Atomic coordinates (x 10^4) and equivalent isotropic displacement parameters ($Å^2$x 10^3) for JFEIX_19. U(eq) is defined as one third of the trace of the orthogonalized U^{ij} tensor.

	x	y	z	U(eq)
Au(1)	2542(1)	2409(1)	1456(1)	16(1)
C(1)	2759(16)	242(12)	-216(7)	71(3)
C(2)	2986(14)	1684(11)	-398(6)	57(2)
C(3)	3557(19)	2288(14)	-1034(8)	77(3)
C(4)	3613(19)	3586(16)	-1147(8)	87(4)
C(5)	3178(15)	4521(13)	-657(6)	68(3)
C(6)	2659(11)	3966(8)	-28(4)	41(2)
C(7)	2224(10)	4897(8)	521(4)	35(2)

C(8)	1782(12)	6289(10)	403(5)	52(2)
C(9)	1439(14)	7112(11)	952(6)	57(2)
C(10)	1557(12)	6652(10)	1600(5)	49(2)
C(11)	1940(9)	5294(7)	1724(4)	32(1)
C(12)	2069(12)	4765(9)	2457(5)	45(2)
Cl(1)	-411(2)	2271(2)	1375(1)	31(1)
Cl(2)	5479(2)	2662(2)	1617(1)	38(1)
Cl(3)	2792(3)	234(2)	1854(1)	47(1)
N(1)	2561(8)	2601(8)	88(3)	40(2)
N(2)	2250(6)	4437(5)	1180(3)	21(1)

Table 3. Bond lengths [Å] and angles [°] for JFEIX_19.

Au(1)-N(2)	2.067(5)
Au(1)-Cl(3)	2.2690(19)
Au(1)-Cl(2)	2.280(2)
Au(1)-Cl(1)	2.2810(19)
Au(1)-N(1)	2.612(6)
C(1)-C(2)	1.471(16)
C(1)-H(1A)	0.9800
C(1)-H(1B)	0.9800
C(1)-H(1C)	0.9800
C(2)-N(1)	1.353(12)

C(2)-C(3)	1.453(18)
C(3)-C(4)	1.294(18)
C(3)-H(3)	0.9500
C(4)-C(5)	1.374(18)
C(4)-H(4)	0.9500
C(5)-C(6)	1.407(14)
C(5)-H(5)	0.9500
C(6)-N(1)	1.362(11)
C(6)-C(7)	1.451(11)
C(7)-N(2)	1.332(9)
C(7)-C(8)	1.422(12)
C(8)-C(9)	1.366(14)
C(8)-H(8)	0.9500
C(9)-C(10)	1.309(14)
C(9)-H(9)	0.9500
C(10)-C(11)	1.381(11)
C(10)-H(10)	0.9500
C(11)-N(2)	1.372(9)
C(11)-C(12)	1.484(11)
C(12)-H(12A)	0.9800
C(12)-H(12B)	0.9800
C(12)-H(12C)	0.9800

N(2)-Au(1)-Cl(3)	174.89(16)
N(2)-Au(1)-Cl(2)	90.79(14)
Cl(3)-Au(1)-Cl(2)	90.24(7)
N(2)-Au(1)-Cl(1)	87.37(14)
Cl(3)-Au(1)-Cl(1)	91.21(7)
Cl(2)-Au(1)-Cl(1)	175.16(7)
N(2)-Au(1)-N(1)	71.8(2)
Cl(3)-Au(1)-N(1)	113.16(18)
Cl(2)-Au(1)-N(1)	91.75(15)
Cl(1)-Au(1)-N(1)	91.94(15)
C(2)-C(1)-H(1A)	109.5
C(2)-C(1)-H(1B)	109.5
H(1A)-C(1)-H(1B)	109.5
C(2)-C(1)-H(1C)	109.5
H(1A)-C(1)-H(1C)	109.5
H(1B)-C(1)-H(1C)	109.5
N(1)-C(2)-C(3)	114.1(10)
N(1)-C(2)-C(1)	116.0(10)
C(3)-C(2)-C(1)	129.9(11)
C(4)-C(3)-C(2)	124.0(14)
C(4)-C(3)-H(3)	118.0
C(2)-C(3)-H(3)	118.0
C(3)-C(4)-C(5)	122.1(15)

C(3)-C(4)-H(4)	119.0
C(5)-C(4)-H(4)	119.0
C(4)-C(5)-C(6)	115.2(12)
C(4)-C(5)-H(5)	122.4
C(6)-C(5)-H(5)	122.4
N(1)-C(6)-C(5)	122.9(8)
N(1)-C(6)-C(7)	118.9(7)
C(5)-C(6)-C(7)	118.2(8)
N(2)-C(7)-C(8)	117.2(7)
N(2)-C(7)-C(6)	118.7(7)
C(8)-C(7)-C(6)	124.1(8)
C(9)-C(8)-C(7)	120.6(9)
C(9)-C(8)-H(8)	119.7
C(7)-C(8)-H(8)	119.7
C(10)-C(9)-C(8)	121.0(11)
C(10)-C(9)-H(9)	119.5
C(8)-C(9)-H(9)	119.5
C(9)-C(10)-C(11)	119.3(9)
C(9)-C(10)-H(10)	120.3
C(11)-C(10)-H(10)	120.3
N(2)-C(11)-C(10)	120.8(7)
N(2)-C(11)-C(12)	119.5(6)
C(10)-C(11)-C(12)	119.6(7)

C(11)-C(12)-H(12A)	109.5
C(11)-C(12)-H(12B)	109.5
H(12A)-C(12)-H(12B)	109.5
C(11)-C(12)-H(12C)	109.5
H(12A)-C(12)-H(12C)	109.5
H(12B)-C(12)-H(12C)	109.5
C(2)-N(1)-C(6)	121.6(8)
C(2)-N(1)-Au(1)	131.1(6)
C(6)-N(1)-Au(1)	103.8(5)
C(7)-N(2)-C(11)	120.9(6)
C(7)-N(2)-Au(1)	123.9(5)
C(11)-N(2)-Au(1)	115.0(4)

Symmetry transformations used to generate equivalent atoms:

Table 4. Anisotropic displacement parameters ($Å^2 x\ 10^3$) for JFEIX_19. The anisotropic displacement factor exponent takes the form: $-2\pi^2[h^2 a^{*2} U^{11} + ... + 2 h k a^* b^* U^{12}]$

	U^{11}	U^{22}	U^{33}	U^{23}	U^{13}	U^{12}
Au(1)	19(1)	11(1)	16(1)	1(1)	0(1)	0(1)
Cl(1)	21(1)	38(1)	34(1)	14(1)	0(1)	-9(1)

Cl(2)	19(1)	37(1)	57(1)	7(1)	-3(1)	3(1)
Cl(3)	56(1)	14(1)	68(1)	11(1)	-8(1)	-1(1)
N(1)	26(3)	74(5)	20(3)	-9(3)	-2(2)	-16(3)
N(2)	19(2)	16(2)	27(2)	8(2)	-8(2)	-3(2)

Table 5. Hydrogen coordinates (x 10^4) and isotropic displacement parameters ($Å^2$x 10^3) for JFEIX_19.

	x	y	z	U(eq)
H(1A)	3328	65	256	107
H(1B)	3280	-334	-560	107
H(1C)	1519	36	-223	107
H(3)	3910	1695	-1388	92
H(4)	3968	3901	-1584	105
H(5)	3224	5475	-737	81
H(8)	1724	6650	-61	63
H(9)	1110	8032	862	69
H(10)	1381	7245	1981	58
H(12A)	1125	4117	2508	67
H(12B)	1980	5522	2787	67
H(12C)	3187	4305	2561	67

Table 6. Torsion angles [°] for JFEIX_19.

N(1)-C(2)-C(3)-C(4)	-2.1(19)
C(1)-C(2)-C(3)-C(4)	176.0(14)
C(2)-C(3)-C(4)-C(5)	2(2)
C(3)-C(4)-C(5)-C(6)	0(2)
C(4)-C(5)-C(6)-N(1)	-1.1(16)
C(4)-C(5)-C(6)-C(7)	178.4(10)
N(1)-C(6)-C(7)-N(2)	19.8(11)
C(5)-C(6)-C(7)-N(2)	-159.7(8)
N(1)-C(6)-C(7)-C(8)	-160.8(8)
C(5)-C(6)-C(7)-C(8)	19.7(13)
N(2)-C(7)-C(8)-C(9)	1.4(13)
C(6)-C(7)-C(8)-C(9)	-178.0(9)
C(7)-C(8)-C(9)-C(10)	1.9(16)
C(8)-C(9)-C(10)-C(11)	-3.6(16)
C(9)-C(10)-C(11)-N(2)	2.0(13)
C(9)-C(10)-C(11)-C(12)	-179.8(9)
C(3)-C(2)-N(1)-C(6)	0.6(14)
C(1)-C(2)-N(1)-C(6)	-177.8(9)
C(3)-C(2)-N(1)-Au(1)	-154.6(8)
C(1)-C(2)-N(1)-Au(1)	27.1(13)

C(5)-C(6)-N(1)-C(2)	0.9(13)
C(7)-C(6)-N(1)-C(2)	-178.5(8)
C(5)-C(6)-N(1)-Au(1)	161.9(8)
C(7)-C(6)-N(1)-Au(1)	-17.6(8)
N(2)-Au(1)-N(1)-C(2)	168.3(8)
Cl(3)-Au(1)-N(1)-C(2)	-13.0(8)
Cl(2)-Au(1)-N(1)-C(2)	78.0(8)
Cl(1)-Au(1)-N(1)-C(2)	-105.2(8)
N(2)-Au(1)-N(1)-C(6)	9.9(5)
Cl(3)-Au(1)-N(1)-C(6)	-171.4(5)
Cl(2)-Au(1)-N(1)-C(6)	-80.4(5)
Cl(1)-Au(1)-N(1)-C(6)	96.5(5)
C(8)-C(7)-N(2)-C(11)	-3.0(10)
C(6)-C(7)-N(2)-C(11)	176.5(6)
C(8)-C(7)-N(2)-Au(1)	171.8(6)
C(6)-C(7)-N(2)-Au(1)	-8.8(9)
C(10)-C(11)-N(2)-C(7)	1.4(10)
C(12)-C(11)-N(2)-C(7)	-176.8(7)
C(10)-C(11)-N(2)-Au(1)	-173.8(6)
C(12)-C(11)-N(2)-Au(1)	8.0(8)
Cl(3)-Au(1)-N(2)-C(7)	-167.7(13)
Cl(2)-Au(1)-N(2)-C(7)	90.8(5)
Cl(1)-Au(1)-N(2)-C(7)	-93.7(5)

N(1)-Au(1)-N(2)-C(7)	-0.8(5)
Cl(3)-Au(1)-N(2)-C(11)	7.4(18)
Cl(2)-Au(1)-N(2)-C(11)	-94.2(4)
Cl(1)-Au(1)-N(2)-C(11)	81.3(4)
N(1)-Au(1)-N(2)-C(11)	174.2(5)

Symmetry transformations used to generate equivalent atoms: